Atomic-Scale Mechanism of Crack-Tip Plasticity: Dislocation Nucleation and Crack-Tip Shielding

Fabrizio Cleri,[1,2] Sidney Yip,[3] Dieter Wolf,[1] and Simon R. Phillpot[1]
[1]*Materials Science Division, Argonne National Laboratory, Argonne, Illinois 60439*
[2]*Divisione Materiali Avanzati, ENEA, Centro Ricerche Casaccia, 00100 Roma A.D., Italy*
[3]*Department of Nuclear Engineering, Massachusetts Institute of Technology, Cambridge, Massachusetts 02139*
(Received 14 April 1997)

By isolating the process of dislocation emission from a crack tip under an applied tensile stress, we extract from a molecular dynamics simulation the atomic-level displacement and stress fields on the activated slip plane before and after the nucleation event. The stress-displacement relations so obtained provide a direct link with recent continuum descriptions of brittle versus ductile behavior in crack propagation. Crack-tip shielding by the emitted dislocations is demonstrated, as is the role of surface steps in dislocation nucleation and crack-tip blunting. [S0031-9007(97)03869-6]

PACS numbers: 61.72.Lk, 61.72.Nn, 62.20.Fe, 62.20.Mk

The brittle versus ductile behavior of materials is still an open problem of both fundamental and technological relevance. While brittle fracture is well understood in terms of the Griffith criterion [1], ductile fracture involves dislocation emission from a crack tip, a complex process of nucleation of a dislocation from the crack surface and its subsequent motion away from the crack [2,3]. Criteria for predicting brittle or ductile behavior [4,5] are usually based on the concept of the energy-release rate (actually an energy per unit area) for cleavage decohesion, G_{cleav}, and dislocation nucleation, G_{disl} (which is usually thought to dominate the emission process, at least in metals). A ductile material is then characterized by $G_{\mathrm{disl}} < G_{\mathrm{cleav}}$, where $G_{\mathrm{cleav}} = 2\gamma_s$, the energy of the two crack surfaces [1].

Recent progress in the continuum approach to the analysis of dislocation nucleation from a crack tip has been achieved by introducing an interplanar potential associated with rigid block sliding in a homogeneous lattice [5–9]. Using heuristic models for this potential, which is equivalent to specifying the stress-displacement constitutive relation on the slip plane, the critical configurations for dislocation nucleation from the crack tip can be calculated, and in this manner estimates of the brittle-to-ductile transition temperature can be made [8,9]. This potential also enables atomic-scale effects to be introduced into the continuum-level description, thus allowing a certain degree of material specificity and providing predictive capability.

Despite the recognized importance of the stress field in the vicinity of a crack tip on dislocation emission, its behavior has not been studied directly by atomistic simulation. Since dislocation emission from a crack tip is a dynamical process which can readily be observed by atomistic simulation [10–13], it follows that one should be able to explicitly extract this information from the atomic-level stresses and displacements given by simulation. In this Letter we show how molecular-dynamics (MD) simulation can produce such an essential input to continuum-model descriptions, as well as provide a test of their validity. Furthermore, our simulations provide insights into the atomic-level mechanisms of dislocation nucleation, crack-tip blunting, and subsequent shielding.

In the following simulations we use a simple Lennard-Jones (LJ) interatomic potential with parameters $\varepsilon = 0.167$ eV and $\sigma = 2.314$ Å, $a_0 = 1.56\sigma$ being the zero-temperature fcc lattice parameter. This model potential, successfully employed in previous simulations of fcc metals [14,15], is cut off smoothly between the fourth- and fifth-nearest neighbors at $1.49a_0$.

The geometry of the three-dimensional (3D) simulation cell is set up corresponding to a number of recent continuum-model crack-tip studies. As shown in Fig. 1, the crack front lies in a (221) plane and runs along the $[1\bar{1}0]$ direction. This choice is made because the (221) plane is representative of a typical fracture surface and has been studied both experimentally and theoretically [6,16]. For this crystal orientation, four {111} slip planes

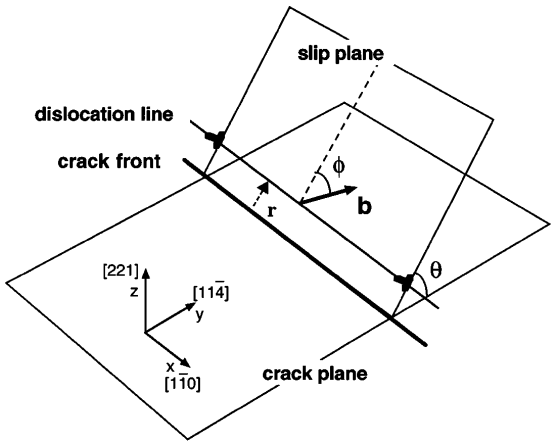

FIG. 1. Geometrical arrangement of a dislocation with Burgers vector b emitted from a crack tip. θ is the inclination angle of the slip plane with respect to the crack plane. ϕ is the angle defining the direction of slip. r is the distance between the crack front and the dislocation line.

intersect the crack front at inclination angles $\theta = 15.8°$, 54.7°, 125.3°, and 164.2°.

In choosing the cell dimensions we have previously shown [17] that the anisotropic continuum-elastic stress field around a microcrack can be well reproduced if the system size L is about 20 crack lengths in the load direction and about 10 crack lengths in the transverse direction. The length of the microcrack is taken to be $6a_0$, thus $L_x = 3a_0$, $L_y = 60a_0$, and $L_z = 120a_0$, corresponding to $N = 86\,400$ atoms in the cell. The cell is taken to be periodic in the x and y directions, while an external tensile load (plane-strain mode I) is applied in the z direction as follows [17]. Prior to inserting the crack, a homogeneous stress σ_{zz} is initially applied by imposing a homogeneous deformation ε_{zz} to a perfect fcc crystal with 3D periodic borders. Plane strain is imposed by keeping L_x fixed while L_y is adjusted so as to relax the lateral stress σ_{yy} to zero. Periodicity along z is then removed, and surface tractions are calculated as the negative of the force on each atom within one cutoff length from the z borders. Then a microcrack is inserted by cutting the interatomic bonds across several selected pairs of atoms [17]. Static lattice relaxation is carried out under the applied surface tractions until a minimum-energy configuration is obtained, with the cut zone opening into an elliptical microcrack. At this point the interactions across the crack surfaces are fully restored: this is the initial configuration for quasistatic MD studies at very low ($T \sim 10^{-3}$ K) temperature. Although this initial configuration is no longer an equilibrium one, we have verified that the time required for the crack tip to adjust to a new quasiequilibrium configuration is about 1 order of magnitude shorter than the typical time over which dislocation nucleation (see below) is initiated.

Figure 2 shows an instantaneous atomic configuration during the simulation at a loading level corresponding to a tensile stress of $\sigma_{zz} = 0.106\mu$, with $\mu = 69.4$ GPa the LJ shear modulus along the $\langle 221 \rangle$ direction. Referring to the initial microcrack (shaded region in Fig. 2), one can see that the crack tips have not advanced, while two stacking faults on the $(11\bar{1})$ planes at $\theta = 54.7°$ have propagated a distance into the bulk. At one end these stacking-fault strips are bounded by a moving partial dislocation, with Burgers vector $b = \frac{1}{6}[112]$ and $\phi = 0°$; at the other end they are bounded by a step on the (221) crack surface. This result demonstrates that our simulation is able to capture the dynamic process of dislocation *emission*, including the *nucleation* from the crack tip and the *motion* away from the crack.

Given this information one can set up a coordinate system (inset of Fig. 3) to obtain the atomic-level displacement field along the slip plane, decomposed into the shear component δ_r and the opening component δ_θ. Figure 3 illustrates the behavior of δ_r as a function of r, the distance from the crack tip along the slip plane (see also Fig. 1), for a sequence of 20 atomic configurations taken at intervals $\Delta t \sim 4$ ps. At any given simulation time during slip along the $(11\bar{1})$ plane, the shear displacement δ_r decreases monotonically with increasing r; i.e., δ_r is always greatest closest to the crack tip. As time increases, all the displacements increase; once the displacement δ_r reaches a value of b, the dislocation core has moved past that particular atom site, and no further displacement occurs. Thus the family of curves in Fig. 3 provides a graphic description of the variation of the shear displacement in time; this constitutes the most detailed (atomic-level) information on dislocation emission from a crack tip. A corresponding family of curves exists for the opening component δ_θ (not shown). These differ from δ_r in two respects. First, the magnitude of δ_θ is smaller by about 1 order of magnitude

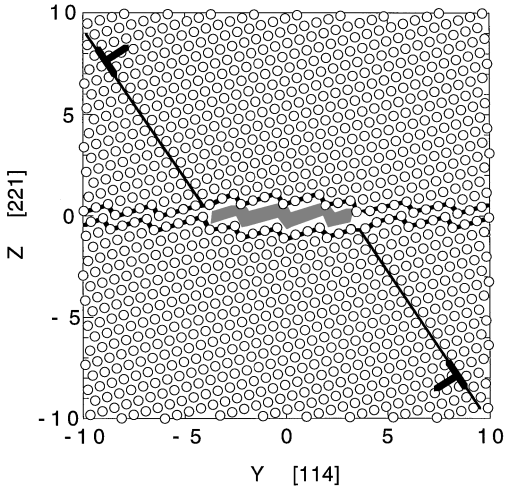

FIG. 2. Central portion of the simulation cell projected onto the y-z plane at the threshold loading level for dislocation emission. The two partial dislocations emitted from the crack tips along the slip planes with $\theta = 54.7°$ are indicated by the straight lines.

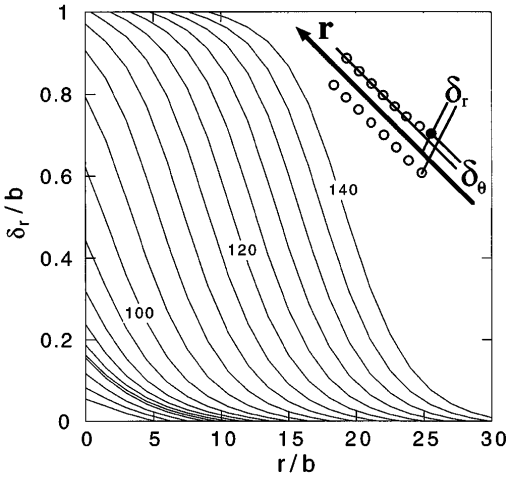

FIG. 3. Displacement component δ_r/b along the slip plane for one of the dislocations in Fig. 2. The curves correspond to simulation times ranging from $t = 60$ ps to $t = 140$ ps, at intervals of 4 ps. Inset: definition of the displacement variables δ_r (shear component) and δ_θ (opening component) for the solid atom.

in comparison to the shear component δ_r. Second, the δ_θ curves show an oscillatory variation with r after a brief initial period.

Using the instantaneous atomic positions and forces one can calculate the atomic-level stress tensor from the well-known virial formula [18], and from this the resolved components on the slip plane of the shear and tensile stresses τ and σ, respectively. The resulting stress fields can be cross-plotted with δ_r and δ_θ, thus generating $\tau(\delta_r)$ and $\sigma(\delta_\theta)$ stress-displacement curves. Figure 4 shows the $\tau(\delta_r)$ curves obtained at different distances $r = 0, 5b$, and $10b$, between the crack tip and the dislocation.

As already mentioned, there has been no previous atomic-level calculation of such stress-displacement relations for dislocation emission from a crack tip. In the first model of a dislocation core by Peierls [19] the sinusoidal function suggested by Frenkel [20] was used. The same sinusoidal form was also recently adopted by Rice in a continuum model of the brittle versus ductile crack-tip behavior [5], and extended to incorporate skewness [8]. One can see in Fig. 4 that the atomistically determined relation is indeed skewed and asymmetric relative to a sinusoid. It is also important to notice that the shear stress at $\delta_r = 0$ and $\delta_r = b$ has an appreciable nonvanishing value. This is because the quantity δ_r defined here (usually referred to as "displacement discontinuity" in continuum models) refers only to that portion of the total displacement associated with the presence of the dislocation; i.e., displacements due to the (purely elastic) lattice response to the applied load prior to the dislocation emission have been subtracted off.

The above stress-displacement relations can now be used to study the energetics of the dislocation nucleation process. The estimate of $G_{\rm disl}$ has been a subject of considerable interest in fracture mechanics [5–9]. In

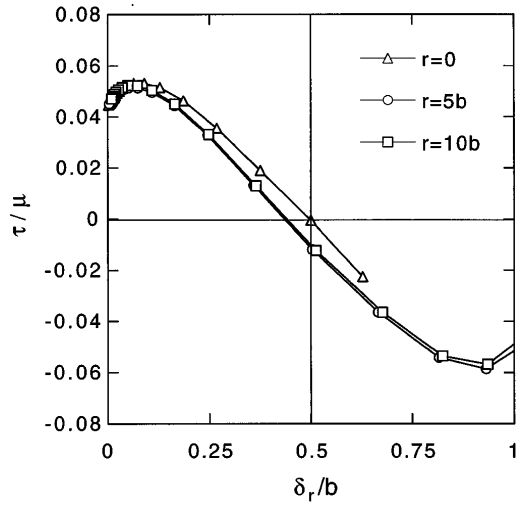

FIG. 4. Shear-displacement curves $\tau(\delta_r)$ for one of the dislocations in Fig. 2, at simulation times corresponding to $r = 0$, $5b$, and $10b$. δ_r is in units of b; τ is in units of the shear modulus μ.

the most recent analysis of Rice [5], the linear-isotropic elasticity approximate form for $G_{\rm disl}$ for a pure edge dislocation is

$$G_{\rm disl} = 8\gamma \frac{1 + (1 - \nu)\tan^2\phi}{(1 + \cos\theta)\sin^2\theta}. \qquad (1)$$

with the angles θ and ϕ as defined in Fig. 1. The quantity γ in Eq. (1) is the energy barrier for dislocation nucleation, generally given by the integral of the (unknown) $\tau(\delta_r)$ curve between $\delta_r = 0$ and the first δ_r at which $\tau = 0$. As a simple approximation, Rice proposed for $\tau(\delta_r)$ the Frenkel-Peierls sinusoidal form and identified γ with $\gamma_{\rm us}$, the "unstable-stacking-fault" energy, equal to the maximum energy obtained during the rigid block sliding along the slip plane of one half of a perfect crystal relative to the other. This approximation implies that the actually nonuniform displacement field on the slip plane in the presence of a nucleating dislocation may be replaced by a uniform displacement distribution corresponding to the rigid block sliding.

Given that in atomistic simulations one can extract detailed information on the energetics and stresses acting on the system, it is possible to test the validity of the uniform-displacements approximation and of the assumption $\gamma = \gamma_{\rm us}$. The minimum applied stress at which dislocation nucleation occurs in our simulations corresponds to a value of $G_{\rm disl} = 0.772\ {\rm J\,m^{-2}}$. For comparison, the much higher value of $G_{\rm disl} = 1.68\ {\rm J\,m^{-2}}$ is obtained from Eq. (1) using the rigid block sliding value of $\gamma_{\rm us} = 0.221\ {\rm J\,m^{-2}}$ for our LJ potential. This discrepancy clearly indicates the inadequacy of the rigid block sliding concept in describing the rapidly varying (i.e., highly inhomogeneous) displacement and stress fields around the dislocation core nucleating from the crack tip. A better approximation to the energy barrier γ for dislocation nucleation, which we call $\gamma_{\rm nucl}$, can be obtained from our simulation by integrating the $\tau(\delta_r)$ curve corresponding to $r = 0$ in Fig. 3, obtaining $\gamma_{\rm nucl} = 0.095\ {\rm J\,m^{-2}}$. When this value of $\gamma = \gamma_{\rm nucl}$ is inserted into Eq. (1), one obtains $G_{\rm disl} = 0.727\ {\rm J\,m^{-2}}$, in much closer agreement with the "directly" observed value.

It is interesting to compare this value for the energy barrier for dislocation nucleation with that for dislocation motion (the well-known Peierls barrier [19]). The latter can be obtained by integrating, as above, the $\tau(\delta_r)$ curves corresponding to $r > 0$, resulting in $\gamma_m = 0.084\ {\rm J\,m^{-2}}$. As could be expected for an fcc metal (despite the limitations of the LJ potential), the barrier for dislocation motion is indeed lower than that for dislocation nucleation, meaning that the latter is the main ductility controlling factor in such systems.

Our simulations also provide insights into crack-tip shielding, the process by which dislocation emission results in relaxation of the stress field around the crack, thereby increasing the critical load for crack propagation. This crack-tip shielding effect can be illustrated by following the time evolution of the partial sum $\sum_i \sigma_{zz}(\mathbf{r}_i)$,

taken over a given volume. Figure 5 shows the time evolution of four such partial sums, extended to all the atoms whose position $\mathbf{r}_i$ is within each one of the four semicircular regions surrounding the two crack tips, depicted in the inset. These regions enclose the dislocation cores throughout the whole simulation described in Fig. 5. It is evident that, as the dislocations move away from the two crack tips, the overall stress level in the two regions containing the dislocations ("up-left" and "down-right" in the figure inset; see also Fig. 2) is continuously reduced relative to the dislocation-free regions, in which the stress remains practically unchanged. As a consequence of this reduction of the crack-tip stress, the effective threshold for crack propagation is increased. Indeed, after dislocation emission the crack does not advance unless the load is increased well above the Griffith critical value $2\gamma_s$; i.e., dislocation emission increases the material toughness.

It has previously been suggested that crack-tip blunting is intimately connected with the formation of a step in the fracture surface immediately at the crack tip [21], in a manner similar to dislocation nucleation from grain-boundary ledges [22] and from stepped surfaces [23]. This connection is clearly revealed by our simulations. As illustrated in Fig. 2, the (221) plane which we have chosen to be the crack surface has a built-in stepped structure consisting of a (4×1) repeat unit formed by segments of the (111) and $(11\bar{1})$ surfaces. These "intrinsic" steps originate from the fact that the (221) surface is vicinal to the atomically flat (111) surface. Detailed examination of the crack surface after the dislocation emission shows that a line defect has been formed on the surface; this line defect is an additional ("extrinsic") step of height $h = b \sin\theta$ which, given $|b| = a_0/\sqrt{6}$ and $\theta = 54.7°$, turns out to be equal to one (221) interplanar spacing, i.e., $h = d(221) = a_0/3$. The blunting of the two crack tips can therefore be attributed to this surface defect formation. These results suggest a scenario for the dislocation-nucleation process which involves a *defect complex* consisting of the embryos of a surface step and a dislocation core to represent the saddle-point configuration for nucleation.

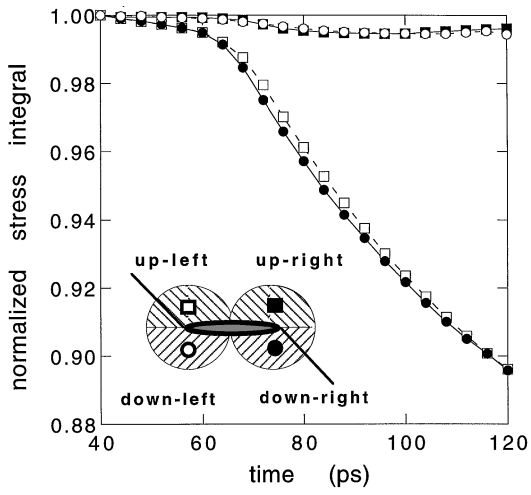

FIG. 5. Integrals of the tensile stress σ_{zz} at the same load of Fig. 2 as a function of the simulation time. Each curve corresponds to one of the semicircular regions shown in the inset, as indicated by the corresponding symbol.

In conclusion, we have shown that atomistic simulations can provide unique insights into the complex physical mechanisms of dislocation nucleation and motion, including crack-tip shielding and blunting. Moreover, atomistic simulations are indeed capable of providing appropriate input to continuum models [5–9], such that quantitatively accurate predictions of brittle versus ductile behavior can be obtained.

The work of F. C., D. W., and S. R. P. was supported by the U.S. Department of Energy, Basic Energy Sciences–Materials Science under Contract No. W-31-109-Eng, and by NATO under Grant No. CRG-950369. The work of F. C. and S. Y. was supported in part by the National Science Foundation under Grant No. PHY94-07194. S. Y. acknowledges support by NSF-MRSEC at MIT and the AFOSR Ceramics Program.

[1] A. A. Griffith, Philos. Trans. R. Soc. London A **221**, 163 (1920).
[2] Y.-H. Chiao and D. R. Clarke, Acta Metall. **47**, 203 (1989).
[3] A. George and G. Michot, Mater. Sci. Eng. A **164**, 118 (1993).
[4] J. R. Rice and R. Thomson, Philos. Mag. **29**, 73 (1974).
[5] J. R. Rice, J. Mech. Phys. Solids **40**, 239 (1992).
[6] G. E. Beltz and J. R. Rice, Acta Metall. Mater. **40**, S321 (1992).
[7] G. Schoeck, Philos. Mag. A **63**, 111 (1991).
[8] G. Xu, A. S. Argon, and M. Ortiz, Philos. Mag. A **72**, 415 (1995).
[9] G. Xu, A. S. Argon, and M. Ortiz, Philos. Mag. A **75**, 341 (1997).
[10] B. De Celis, A. S. Argon, and S. Yip, J. Appl. Phys. **54**, 4864 (1983).
[11] K. S. Cheung and S. Yip, Phys. Rev. Lett. **65**, 2804 (1990).
[12] F. F. Abraham *et al.*, Phys. Rev. Lett. **73**, 272 (1994).
[13] S. J. Zhou *et al.*, Phys. Rev. Lett. **78**, 479 (1997).
[14] D. Wolf and J. F. Lutsko, J. Mater. Res. **4**, 1427 (1989).
[15] D. Wolf and K. Merkle, in *Materials Interfaces*, edited by D. Wolf and S. Yip (Chapman and Hall, London, 1992), p. 87.
[16] J.-S. Wang and P. M. Anderson, Acta Metall. Mater. **39**, 779 (1991).
[17] F. Cleri *et al.*, in *Advances in Computational Materials Science*, edited by V. Fiorentini and F. Meloni (Societa' Italiana di Fisica, Bologna, 1997) p. 71.
[18] M. P. Allen and D. J. Tildesley, *Computer Simulations of Liquids* (Oxford Science Publications, Oxford, 1989).
[19] R. E. Peierls, Proc. Phys. Soc. **52**, 34 (1940).
[20] J. Frenkel, Z. Phys. **37**, 572 (1926).
[21] S. J. Zhou, A. E. Carlsson, and R. Thomson, Phys. Rev. Lett. **72**, 852 (1994).
[22] J. C. M. Li, Trans. Metall. Soc. AIME **227**, 239 (1963).
[23] L. G. Orlov, Sov. Phys. Solid State **9**, 1836 (1968).